

B.S. LUK¹ YANCHUK^{1,✉}
M.I. TRIBELSKY²
Z.B. WANG³
Y. ZHOU¹
M.H. HONG¹
L.P. SHI¹
T.C. CHONG¹

Extraordinary scattering diagram for nanoparticles near plasmon resonance frequencies

¹ Data Storage Institute, Agency for Science, Technology and Research, 117608 Singapore
² Moscow State Institute of Radioengineering, Electronics and Automation, Moscow 119454, Russia
³ School of Mechanical, Aerospace and Civil Engineering, University of Manchester, Manchester, M60 1QD, UK

Received: 2 February 2007/Accepted: 2 May 2007
Published online: 21 June 2007 • © Springer-Verlag 2007

ABSTRACT Light scattering by a small spherical particle with low dissipation rate is discussed according to the Mie theory. It is shown that near plasmon (polariton) resonance frequencies one can see non-Rayleigh anomalous light scattering with quite unusual scattering diagrams.

PACS 42.25.Fx; 42.65.Es; 46.40.Ff; 78.67.Bf

1 Introduction

According to the Rayleigh approximation a small particle scatters light as a point dipole. The dipole far field scattering polar diagram is presented by the well known “8-shaped” distribution, which has been discussed in many books, see e.g. [1, 2]. Although the dipole scattering paradigm for small particles has existed for more than 100 years, it was shown recently that the Rayleigh approximation fails for a particular case of weakly dissipating materials near plasmon (polariton) resonance frequencies. One can see immediately that the Rayleigh scattering cross-section contains an $\varepsilon + 2$ factor in the denominator and diverges if $\text{Re}\varepsilon = -2$ and $\text{Im}\varepsilon \rightarrow 0$, where $\varepsilon = \varepsilon_p/\varepsilon_m$ is the relative dielectric permittivity; ε_p and ε_m stand for the dielectric permittivities of the particle and media, respectively. Note however, that optical excitation of localized plasmons is accompanied by an inverse process – transformation of localized resonant plasmons into scattered light, resulting in the radiative damping, see e.g. [3, 4]. The Rayleigh approximation holds when this radiative damping is small compared to the usual dissipative one. In the opposite limit, when the radiative damping prevails, the Rayleigh scattering is replaced by the anomalous light scattering [5], which results in sharp giant optical resonances and a complicated near-field structure of the Poynting vector field [5–8]. Here we demonstrate that the anomalous light scattering is characterized by an extraordinary scattering diagram, where a small variation in the incident light frequency changes the scattering diagram completely, e.g. from forward scattering to backward scattering. This effect can be used in data storage technologies and some other applications.

2 Theoretical model

In fact this extraordinary scattering effect follows from the classical Mie theory [1, 2]. We just consider the range of parameters of the Mie solution, which usually is not inspected. In the far field $r \gg \lambda$ (r is the distance from the particle center), the radial component of the scattered radiation is negligible and the scattered diagram is defined by angular components $|E_\theta^{(s)}|^2 = I_{\text{II}}^{(s)} \cos^2 \varphi$ and $|E_\varphi^{(s)}|^2 = I_{\perp}^{(s)} \sin^2 \varphi$, where the corresponding scattering intensities are presented by the asymptotic of the Mie formulas (see e.g. formula (98) in Chapter XIV [1]):

$$I_{\text{II}}^{(s)} = \frac{a^2}{r^2 q^2} \left| \sum_{\ell=1}^{\infty} (-1)^\ell \times \left[{}^e B_\ell P_\ell^{(1)'}(\cos \theta) \sin \theta - {}^m B_\ell \frac{P_\ell^{(1)}(\cos \theta)}{\sin \theta} \right] \right|^2,$$
$$I_{\perp}^{(s)} = \frac{a^2}{r^2 q^2} \left| \sum_{\ell=1}^{\infty} (-1)^\ell \times \left[{}^e B_\ell \frac{P_\ell^{(1)}(\cos \theta)}{\sin \theta} - {}^m B_\ell P_\ell^{(1)'}(\cos \theta) \sin \theta \right] \right|^2. \quad (1)$$

Here $P_\ell^{(1)}(\cos \theta)$ are the associated Legendre polynomials, and the stroke indicates differentiation over the entire argument of the corresponding function, i.e. $P_\ell^{(1)'}(z) \equiv dP_\ell^{(1)}(z)/dz$. Quantity $q = 2\pi a \sqrt{\varepsilon_m}/\lambda \equiv a\omega \sqrt{\varepsilon_m}/c$ defines the so called size parameter, λ is the wavelength of the incident light in vacuum, ω is its frequency, c is the speed of light in vacuum, and a is the radius of the spherical particle. The scattering amplitudes ${}^e B_\ell$ (electric) and ${}^m B_\ell$ (magnetic) within the framework of the Mie theory are given by the following expressions:

$${}^e B_\ell = i^{\ell+1} \frac{2\ell+1}{\ell(\ell+1)} a_\ell, \quad {}^m B_\ell = i^{\ell+1} \frac{2\ell+1}{\ell(\ell+1)} b_\ell, \quad (2)$$

where

$$a_\ell = \frac{\mathfrak{R}_\ell^{(a)}}{\mathfrak{R}_\ell^{(a)} + i\mathfrak{I}_\ell^{(a)}}, \quad b_\ell = \frac{\mathfrak{R}_\ell^{(b)}}{\mathfrak{R}_\ell^{(b)} + i\mathfrak{I}_\ell^{(b)}}, \quad (3)$$

$$\begin{aligned}\Re_{\ell}^{(a)} &= n\psi'_{\ell}(q)\psi_{\ell}(nq) - \psi_{\ell}(q)\psi'_{\ell}(nq), \\ \Im_{\ell}^{(a)} &= n\chi'_{\ell}(q)\psi_{\ell}(nq) - \psi'_{\ell}(nq)\chi_{\ell}(q),\end{aligned}\quad (4)$$

and

$$\begin{aligned}\Re_{\ell}^{(b)} &= n\psi'_{\ell}(nq)\psi_{\ell}(q) - \psi_{\ell}(nq)\psi'_{\ell}(q), \\ \Im_{\ell}^{(b)} &= n\chi_{\ell}(q)\psi'_{\ell}(nq) - \psi_{\ell}(nq)\chi'_{\ell}(q).\end{aligned}\quad (5)$$

Here $\psi_{\ell}(z) = \sqrt{\frac{\pi}{2}}J_{\ell+\frac{1}{2}}(z)$, $\chi_{\ell}(z) = \sqrt{\frac{\pi}{2}}N_{\ell+\frac{1}{2}}(z)$, where $J_{\ell}(z)$ and $N_{\ell}(z)$ are the Bessel and the Neumann functions, respectively. The strokes in formulas (4), (5) once again indicate differentiation over the entire argument of the corresponding functions, i.e. $\psi'_{\ell}(z) \equiv d\psi_{\ell}(z)/dz$, etc.; $n = \sqrt{\varepsilon}$ is the relative complex refraction index. We consider the same geometry as that in [1], i.e. the incident plane wave with unity amplitude propagates along the z -axis, the electric vector directed along the x -coordinate and the magnetic vector along the y -coordinate. Spherical coordinates are r , θ and φ , where θ is the azimuthal angle between the radius vector \mathbf{r} and the z -axis, φ is the polar angle at x , y -plane.

The extinction, scattering and absorption cross-sections are given by the expression $\sigma = \pi a^2 Q$, where related efficiencies Q are presented by amplitudes a_{ℓ} and b_{ℓ} as follows [1, 2]:

$$Q_{\text{ext}} = \frac{2}{q^2} \sum_{\ell=1}^{\infty} (2\ell+1) \operatorname{Re}(a_{\ell} + b_{\ell}), \quad (6)$$

$$Q_{\text{sca}} = \frac{2}{q^2} \sum_{\ell=1}^{\infty} (2\ell+1) \{ |a_{\ell}|^2 + |b_{\ell}|^2 \}, \quad (7)$$

$$Q_{\text{abs}} = Q_{\text{ext}} - Q_{\text{sca}}. \quad (8)$$

We want to draw attention to the fact that formulas (1)–(5) follow from the exact solution of the Maxwell equations and they are valid for any size parameter q and any dielectric function ε . The only approximation done so far is that in (1), which is valid for far field scattering only. However, at small q (2)–(8) may be simplified too, namely by expanding the Bessel and Neumann functions in power series, one can find at small q [9]:

$$\Re_{\ell}^{(a)} \approx q^{2\ell+1} \frac{(\ell+1)}{[(2\ell+1)!!]^2} n^{\ell} (n^2 - 1), \quad (9)$$

$$\begin{aligned}\Im_{\ell}^{(a)} \approx n^{\ell} \frac{\ell}{2\ell+1} &\left[n^2 + \frac{\ell+1}{\ell} - \frac{q^2}{2} (n^2 - 1) \right. \\ &\times \left. \left(\frac{n^2}{2\ell+3} + \frac{\ell+1}{\ell(2\ell-1)} \right) \right],\end{aligned}\quad (10)$$

$$\Re_{\ell}^{(b)} \approx -\frac{nq^2}{2\ell+1} \Re_{\ell}^{(a)}, \quad (11)$$

$$\Im_{\ell}^{(b)} \approx -n^{\ell+1} \left[1 + \frac{1-n^2}{2(2\ell+1)} q^2 \right]. \quad (12)$$

Far from the resonances $\Re \ll \Im$. In this case the term with $\ell = 1$ (dipole scattering) plays the dominant role. Also for small particles one can neglect magnetic amplitudes compared to the electric ones because of their additional smallness in q . Thus, the amplitude $a_1 \approx -\frac{2i}{3} \frac{\varepsilon-1}{\varepsilon+2} q^3$ plays the dominant role. It yields the classical Rayleigh formula:

$$Q_{\text{sca}} \approx \frac{8}{3} \left| \frac{\varepsilon-1}{\varepsilon+2} \right|^2 q^4. \quad (13)$$

As we have mentioned above this formula has singularity at the plasmon resonance frequency, when $\varepsilon = -2$. In reality this divergence does not exist; it is stabilized either by dissipative processes or by the radiative damping at low dissipation rates. One can see immediately from the exact (3) that for nondissipative media maximal values of the amplitudes are $a_{\ell} = 1$ and $b_{\ell} = 1$ at plasmon resonance frequencies, where $\Im_{\ell}^{(a)}(q, \varepsilon(\omega_{\ell}^{(a)})) = 0$ (electric resonance) and $\Im_{\ell}^{(b)}(q, \varepsilon(\omega_{\ell}^{(b)})) = 0$ (magnetic resonance), respectively. For small particles and $\varepsilon \leq -1$ only electric resonances occur. Therefore in what follows, a simplified notation ω_{ℓ} is employed to denote $\omega_{\ell}^{(a)}$. Thus, the scattering efficiency for a nondissipative particle at exact resonance frequencies ω_{ℓ} is given by the expression

$$Q_{\text{sca}} \approx Q_{\text{sca}}^{(\ell)} = 2(2\ell+1)/q^2, \quad (14)$$

where $Q_{\text{sca}}^{(\ell)}$ stands for the partial scattering efficiency. Equation (14) is valid for resonances, which do not overlap significantly. Thus, this formula is applicable up to $q \approx 1$. As in the vicinity of the resonances at $q \ll 1$ the net efficiency is overwhelmingly determined by the corresponding partial one, the expression (14) means that the resonance scattering cross section increases with an increase in the order of the resonance ℓ . For example, the cross-section at the quadrupole resonance is 5/3 of that at the dipole resonance, etc.. This “inverse hierarchy of resonances” [4, 5] is a remarkable feature, which disagrees with the conventional Rayleigh case dramatically. Equation (14) also exhibits inverse frequency dependence – while in the Rayleigh case the scattering cross-section increases with an increase of frequency ($q \propto \omega$) as ω^4 , see (13), in the case given by (14) it decreases¹ as ω^{-2} . Note also that the corresponding resonant cross-section $\sigma_{\text{sca}}^{(\ell)} = \frac{2\pi}{\varepsilon_m} \frac{c^2}{\omega_{\ell}^2} (2\ell+1)$ does not depend on the particle size and therefore does not vanish at $a \rightarrow 0$. The finiteness of the cross-section for a particle with zero radius obviously is an artifact related to the non-dissipative limit [4, 5, 10]. In reality there is competition between the radiative damping and the one related to the dissipative losses. All the fascinating effects discussed are strongly suppressed by dissipation. The necessary conditions for the anomalous scattering to take place may be found from the Mie theory, taking into account the dissipation factor ε'' in the denominator of the scattering amplitude. This consideration leads to the applicability condition [4, 5]

$$\varepsilon''(\omega_{\ell}) \ll \frac{q^{2\ell+1}}{\ell [(2\ell-1)!!]^2}. \quad (15)$$

When this condition is fulfilled the anomalous scattering is dominant. In the opposite case the Rayleigh scattering is restored. The condition clearly explains numerical results found in [10]. For example, it follows from (15) that with any small but finite ε'' the anomalous scattering is suppressed for very small particles. Thus, under real experimental conditions the

¹ It should be stressed however, that while in the Rayleigh case ω may take any values, for the anomalous scattering ω should belong to the close vicinity of the corresponding resonance frequency. The latter is determined by the condition $\Im_{\ell}^{(a)}(q, \varepsilon(\omega_{\ell})) = 0$ for each order of resonance ℓ .

anomalous scattering can be realized just in some intermediate range of size parameter and only up to a certain order of the resonances: $\ell < \ell_{\max}$. We can illustrate this effect for metal, whose dielectric permittivity is described by the Drude formula:

$$\varepsilon = n^2 = 1 - \frac{\omega_p^2}{\omega^2 + \gamma^2} + i \frac{\gamma}{\omega} \frac{\omega_p^2}{\omega^2 + \gamma^2}. \quad (16)$$

Here, as usual, ω_p denotes the plasma frequency, while γ is the frequency of electron collisions. Introducing normalized frequency $\tilde{\omega} = \omega/\omega_{sp}$ and normalized collision frequency $\tilde{\gamma} = \gamma/\omega_{sp}$, where $\omega_{sp} = \omega_p/\sqrt{3}$ stands for the frequency of the dipole surface plasmon resonance at $q \rightarrow 0$, one can rewrite (16) as follows:

$$\varepsilon = 1 - \frac{3}{\tilde{\omega}^2 + \tilde{\gamma}^2} + i \frac{\tilde{\gamma}}{\tilde{\omega}} \frac{3}{\tilde{\omega}^2 + \tilde{\gamma}^2}. \quad (17)$$

In Fig. 1 the corresponding resonances are shown for the nondissipative limit $\gamma = 0$ and for the cases of weak dissipation with $\tilde{\gamma} = 10^{-2}$ and 10^{-3} , respectively. The inverse hierarchy of resonances exists for the nondissipative limit although even small dissipation suppresses this effect for small q . However at $q = 0.7$ and $\tilde{\gamma} = 10^{-3}$ the effect is still pronounced at $\ell = 2$.

3 Results and discussions

Now we can return to the scattering diagram in (1). Following [1] we will present the scattering diagram in the xz -plane ($\varphi = 0$) as a function of angle θ for two cases: linearly polarized light and nonpolarized light. The first case corresponds to the situation when the length of radius vector $I_{II}^{(s)}(\theta)$ presents the corresponding intensity. For nonpolarized light we can consider averaging $\langle \cos^2 \varphi \rangle = \langle \sin^2 \varphi \rangle = 1/2$; thus, the length of radius vector $I_{II}^{(s)}(\theta) + I_{\perp}^{(s)}(\theta)$ presents the

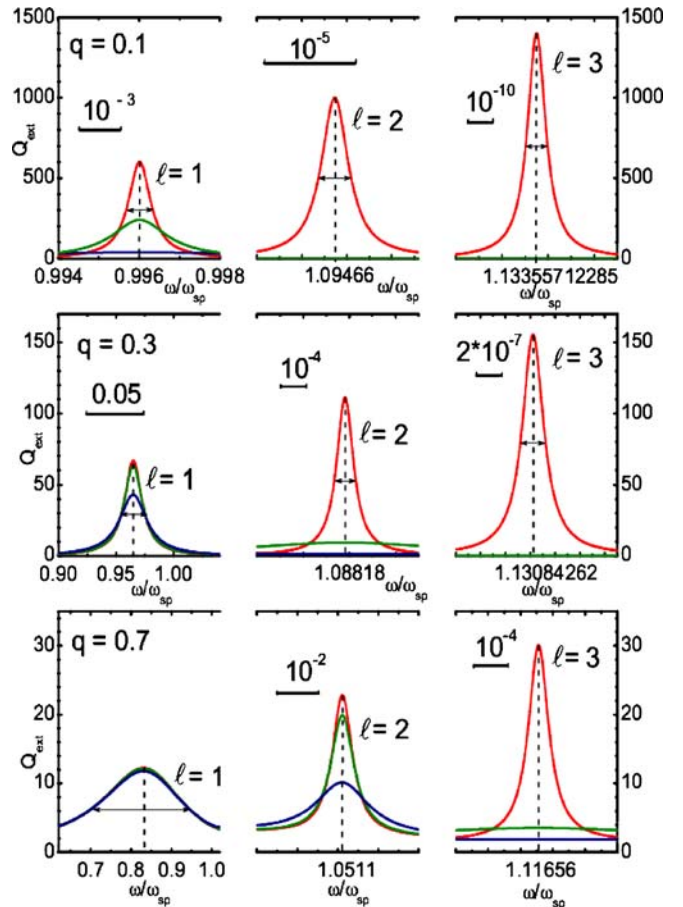


FIGURE 1 The exact Mie solution; dependencies of extinction efficiency at characteristic frequencies of dipole ($\ell = 1$), quadrupole ($\ell = 2$) and octopole ($\ell = 3$) resonances at three different values of the size parameter: $q = 0.1, 0.3$ and 0.7 , respectively. Lines with different colours correspond to nondissipative case $\gamma = 0$ (red), $\tilde{\gamma} = 10^{-3}$ (olive) and $\tilde{\gamma} = 10^{-2}$ (navy). For $\tilde{\gamma} = 10^{-3}$ and $q = 0.7$ one can see an inverse hierarchy – the quadrupole resonance is stronger than the dipole. The resonances for the nondissipative limit are extremely sharp, e.g. for $q = 0.1$ the width of the octopole resonance is 10^{-10} of the characteristic resonance frequency and the corresponding cross-section of extinction exceeds the geometric cross-section in three orders of magnitude

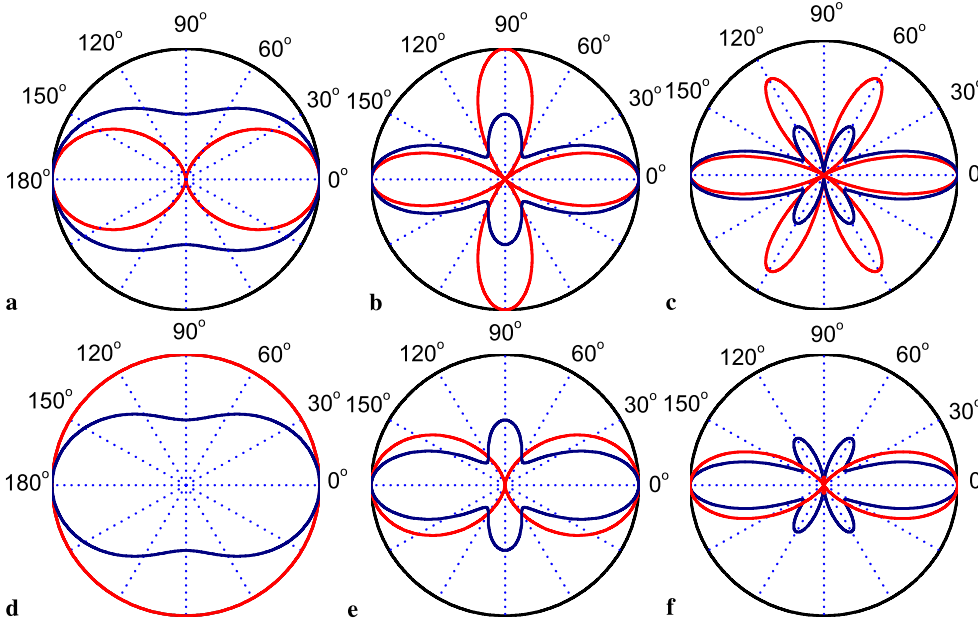


FIGURE 2 The exact Mie solution; polar diagrams in the xz -plane ($\varphi = 0$) for the electric dipole $\ell = 1$ (a), quadrupole $\ell = 2$ (b) and octopole $\ell = 3$ (c) plasmon resonances according to (18)–(20). Analogous diagrams in the xz -plane for magnetic resonances with $\ell = 1, 2$ and 3 are shown in plots (d), (e) and (f). Red lines correspond to linearly polarized light, navy to nonpolarized

corresponding intensity. In the case of the Rayleigh scattering amplitude a_1 plays the dominant role. Thus,

$$I_{\text{II}}^{(1)}(\theta) = \frac{a^2}{r^2} \frac{1}{q^2} |a_1|^2 \frac{9}{4} \cos^2 \theta, \quad I_{\perp}^{(1)}(\theta) = \frac{a^2}{r^2} \frac{1}{q^2} |a_1|^2 \frac{9}{4}. \quad (18)$$

This produces the universal “8-shaped” (or ∞ - shaped depending on the definition of angle θ) angular distribution, which does not depend on the size parameter (at $q \ll 1$) or dielectric permittivity ϵ , see Fig. 2. Only the total intensity depends on these parameters. With anomalous light scattering the polar diagram remains the same, one should only put $a_1 = 1$ in the formulas in Eq. (18). The important point however is that for the anomalous light scattering we also have pronounced higher order resonances for a small particle, e.g. quadrupole and octopole resonances shown in Fig. 1, while in the case of the Rayleigh scattering they are suppressed. At $q \ll 1$ these resonances are not overlapped and they have polar diagrams, which are presented at exact resonance frequencies by (1) with a single term, e.g. with $a_2 = 1$ for quadrupole resonance, or with $a_3 = 1$ for octopole resonance, etc., namely:

$$I_{\text{II}}^{(2)}(\theta) = \frac{a^2}{r^2} \frac{1}{q^2} |a_2|^2 \frac{25}{4} \cos^2 2\theta, \\ I_{\perp}^{(2)}(\theta) = \frac{a^2}{r^2} \frac{1}{q^2} |a_2|^2 \frac{25}{4} \cos^2 \theta, \quad (19)$$

$$I_{\text{II}}^{(3)}(\theta) = \frac{a^2}{r^2} \frac{1}{q^2} |a_3|^2 \frac{49}{1024} (\cos \theta + 15 \cos 3\theta)^2, \\ I_{\perp}^{(3)}(\theta) = \frac{a^2}{r^2} \frac{1}{q^2} |a_3|^2 \frac{49}{256} (3 + 5 \cos 2\theta)^2. \quad (20)$$

For pure magnetic resonances (which occur at non-small q) the scattering diagrams are produced by the corresponding terms, related to magnetic amplitudes b_ℓ . To obtain the scattering intensities in this case one has to replace $a_\ell \rightarrow b_\ell$, and $I_{\text{II}}^{(\ell)}(\theta) \leftrightarrow I_{\perp}^{(\ell)}(\theta)$ in the expressions for the electric resonances discussed above. Thus, the scattering diagrams for

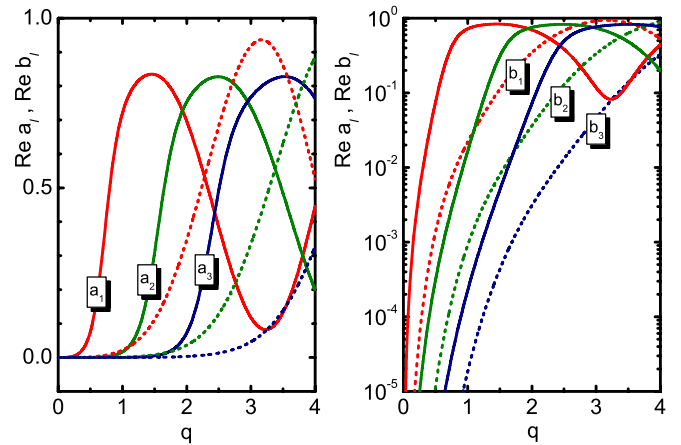
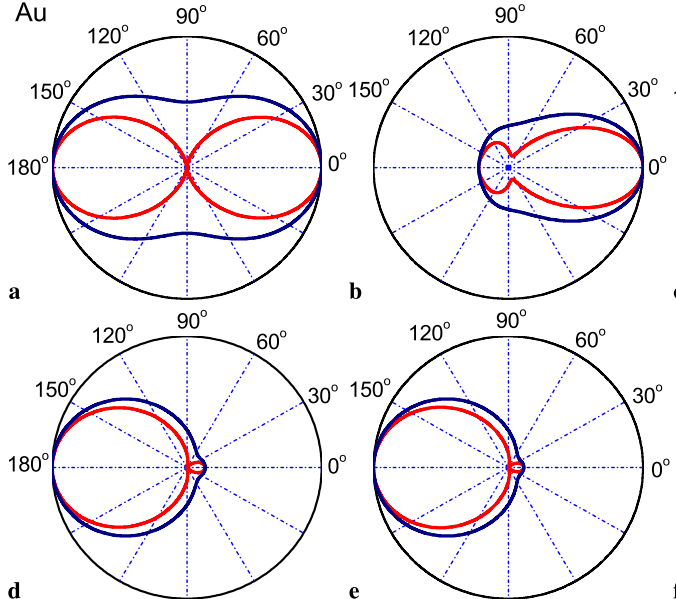


FIGURE 3 The exact Mie solution; amplitudes of the first three electrical a_ℓ (solid lines) and magnetic b_ℓ (dash lines) resonances for gold nanoparticles in water for the radiation wavelength $\lambda = 550$ nm. We used data of [1]: for water $n_m = \sqrt{\epsilon_m} = 1.33$ and for Au $n_p = \sqrt{\epsilon_p} = 0.57 + i2.45$. Different electric and magnetic resonances overlap in the range of non-small size parameters $q \approx 1$ (or larger), which can be seen well in the *right plot* with a logarithmic scale

magnetic resonances in the yz -plane ($\varphi = \pi/2$) are obtained from the ones for the electric resonances in the xz -plane ($\varphi = 0$), etc. Polar diagrams for the first three electric and magnetic resonances are shown in Fig. 2.

For strongly dissipating (at the resonance frequencies) materials, e.g. for gold, amplitudes of partial resonances for small particle $q \ll 1$ are small $a_{i+1} \ll a_i \ll 1$ while the widths of the resonances are quite large. Different electric and magnetic resonances overlap in the range of non-small size parameters $q \approx 1$ (or larger), see in Fig. 3. Overlapping of different resonances and their interference produce more complicated scattering diagrams, see (1). Some examples of that for gold nanoparticle are presented in Fig. 4.

With perfectly conducting material (conductivity $\sigma \gg \omega$) or very large dielectric constant (refractive index $n_p \gg 1$) the particle mostly produces backward scattering (“reflected” ra-

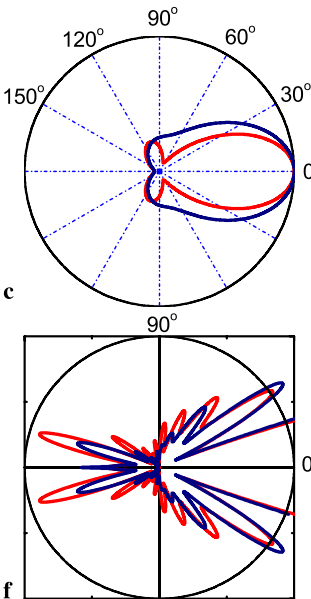


FIGURE 4 The exact Mie solution; scattering diagram for a gold particle, $n_p = 0.57 + i2.45$, in water, $n_m = 1.33$, for radiation wavelength $\lambda = 550$ nm. The radius of the particle $a = 8.75$ nm (a), 80 nm (b) and 90 nm (c), respectively. Similar diagrams are shown in Fig. 14.10 of [1]. The corresponding size parameter $q = 2\pi a n_m / \lambda$ equals 0.133 (a), 1.215 (b) and 1.367 (c). Plot (d) presents a scattering diagram for a small particle $a = 8.75$ nm of highly conducting material $\epsilon_p = \sqrt{14\pi\sigma/\omega}$, $\sigma/\omega = 10^4$. Plot (e) represents a similar diagram for the particle with a large value of refractive index $n_p = 100$. The last picture (f) represents details of the scattering diagram for a large particle with $q = 10$ and refractive index $n_p = 1.5$. We consider vacuum as surrounding media, $n_m = 1$, in the plots (d), (e) and (f). Red and navy lines have the same meaning as that in Fig. 2

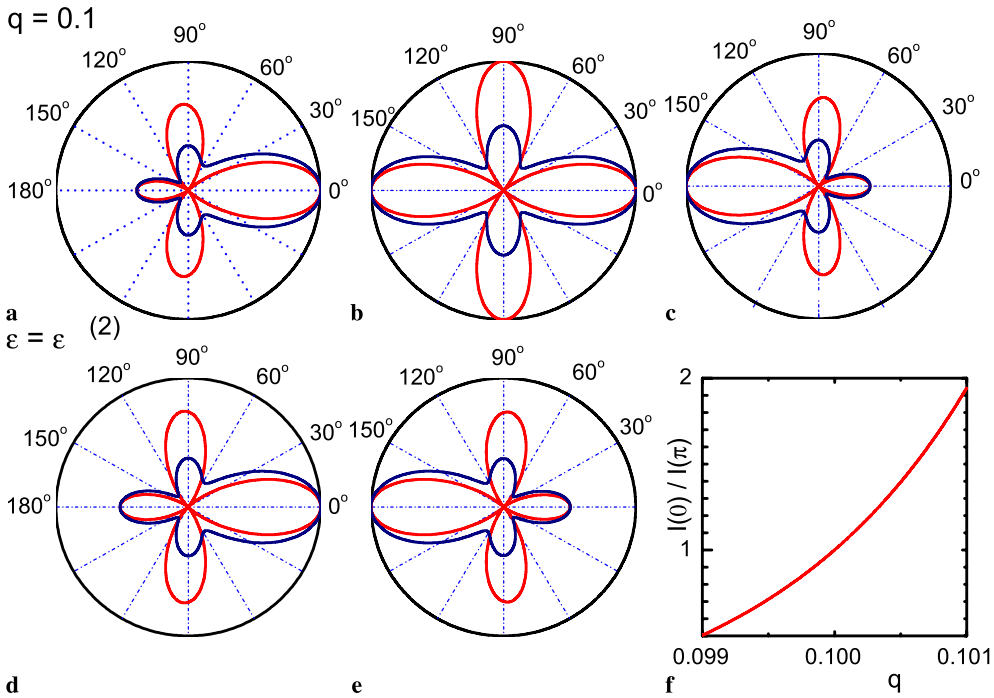


FIGURE 5 The exact Mie solution; variation in the scattering diagram near quadrupole resonance for the particle with $q = 0.1$. For nondissipative materials it corresponds to dielectric permittivity $\epsilon = \epsilon^{(2)} = -1.503588$. The left plot shows the scattering diagram for $\epsilon = \epsilon^{(2)} + 10^{-4}$ (a), the central plot – for exact resonance (b), and the right plot – for $\epsilon = \epsilon^{(2)} - 10^{-4}$ (c). With this small change in ϵ the scattering diagram varies from forward scattering to backward scattering. Pictures (d) and (e) are calculated for fixed $\epsilon = \epsilon^{(2)}$ but the particle size changes for 1%: $q = 0.101$ (d) and $q = 0.099$ (e). Plot (f) shows the ratio of forward to backward scattering intensities with a small variation of the size parameter

diation). In these cases in spite of small $q = 2\pi a \sqrt{\epsilon_m} / \lambda$, the size parameter for the particle $q_p = 2\pi a \sqrt{\epsilon_p} / \lambda$ cannot be considered as a small quantity and (9)–(12) are not valid anymore. Inspection of the case of ideally reflected small sphere, $\sigma/\omega \rightarrow \infty$ shows the ratio of forward and backscattered intensities of 1:9, see Problem 2 to § 92 in [11]. When both parameters q and q_p are small, the Rayleigh scattering yields the symmetrical diagram, shown in Fig. 4a. As the radius of the sphere increases to $q \approx 1$, more light is scattered in the forward direction (the so-called Mie effect [1], see Fig. 4b,c).

The anomalous light scattering for weakly dissipating materials at $q \ll 1$ also presents the situation when different resonances may interfere with each other. Although at the exact resonance the net scattering diagram is overwhelmingly determined by the corresponding partial diagram, shown in Fig. 2, small detuning out of the resonance frequency yields comparable partial scattering amplitudes for different modes. It means that near the partial plasmon resonance frequencies the scattering diagram have extra fast modifications, see Fig. 5 as an example. Similar effects arise also with a small variation of the particle size at fixed light frequency. We call these diagrams extraordinary scattering diagrams. The extreme sensitivity of the diagram presented in Fig. 5 to the finest variations in ϵ is related to the non-dissipative limit. Finite dissipation smoothes the effect, though the effect exists as long as the corresponding high order resonances remain pronounced.

Strong variations in scattered intensities can be found at different angles. Thus, weakly dissipating materials have a very high dispersion of polarization. This effect can be used for different applications, e.g. optical recording. Also small temperature variations in ϵ can lead to high dispersion in polarization. However it should be stressed that to have the effect pronounced one needs materials with weak dissipation near plasmon resonance frequencies. A possible candidate which might exhibit the discussed modifications in polar scatter-

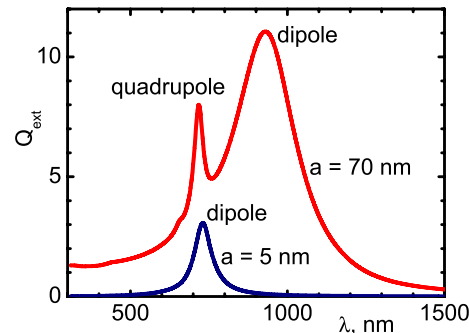


FIGURE 6 The exact Mie solution; spectral dependencies of the extinction efficiency for a potassium cluster in a KCl matrix. Optical constants for both materials are taken from [13]. In our calculations we took into account the size effect renormalizing the collision frequency of free electrons due to their collisions with particle surface [14], $\gamma \rightarrow \gamma_\infty + v_F/a$. The data for the Fermi velocity $v_F = 8.6 \times 10^7$ cm/s for this renormalization was taken from [12]

ing diagram near quadrupole resonance might be an additively colored alkali halide crystal (those with a stoichiometric excess of the alkali component), e.g. potassium chloride. A small metal cluster of potassium produces the dipole scattering with the peak position at 730 nm [12]. It agrees with our calculations, see Fig. 6. The quadrupole resonance cannot be seen for a very small cluster because of its suppression by dissipation, see (15). However this resonance becomes pronounced at larger values of the size parameter, as we have discussed above, see also Fig. 1. For example for a cluster with $a = 70$ nm the quadrupole resonance is quite pronounced and for $a > 90$ nm (in some range of sizes) the amplitude of this resonance is larger than that for the dipole resonance.

4 Conclusion

One can see in Fig. 7 that the shape of the scattering diagram practically does not change with variation of the

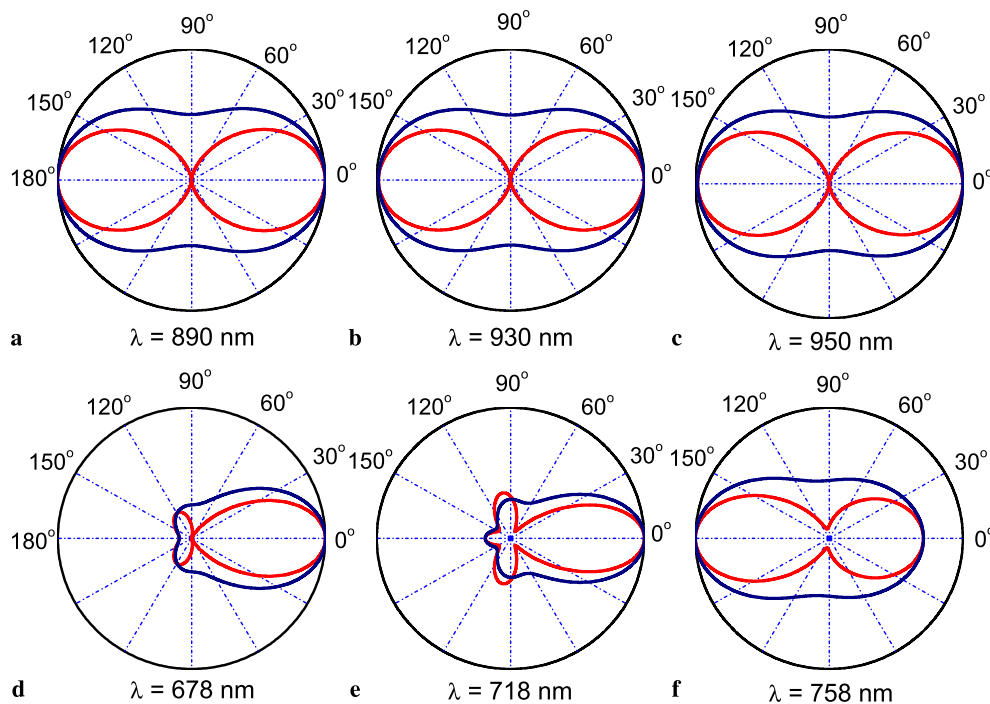


FIGURE 7 Scattering diagram near dipole (**a–c**) and quadrupole (**d–f**) resonances for a potassium spherical nanocluster with radius $a = 70$ nm immersed in a KCl matrix

incident light wavelength in the vicinity of the dipole resonance (peak at 930 nm), but does change dramatically with its variation in the vicinity of the quadrupole resonance (peak at 718 nm) from forward at $\lambda = 718$ nm to basically backward scattering at $\lambda = 758$ nm. This clearly indicates the mentioned dispersion of polarization near the quadrupole resonance for weakly dissipating materials.

An extraordinary scattering diagram can be also found for sodium nanoclusters immersed in a NaCl matrix, as well as for aluminium nanoclusters in vacuum. Many researchers (see Refs. in [12]) have reported that the thermal heating-cooling process yields variation of the size of alkali-metal colloidal particles in the additively colored alkali halide crystals. Because of the extraordinary scattering effect this permits the use of the dispersion of polarization to write and read multi-bit information in nanoclusters with sub 100 nm range of sizes.

ACKNOWLEDGEMENTS We are very thankful to S.I. Anisimov, L.P. Pitaevskiy and N. Arnold for discussions and critical comments. This work was partially supported by the Russian Basic Research Foundation (grant 070200764-a).

REFERENCES

- 1 M. Born, E. Wolf, *Principles of Optics*, 7th edn. (University Press, Cambridge, 1999)
- 2 C.F. Bohren, D.R. Huffman, *Absorption and Scattering of Light by Small Particles* (Wiley, New York, 1998)
- 3 R. Fuchs, K.L. Kliewer, J. Opt. Soc. Am. **58**, 319 (1968)
- 4 M.I. Tribelsky, Sov. Phys. JETP **59**, 534 (1984)
- 5 M.I. Tribelsky, B.S. Luk'yanchuk, Phys. Rev. Lett. **97**, 263902 (2006)
- 6 Z.B. Wang, B.S. Luk'yanchuk, M.H. Hong, Y. Lin, T.C. Chong, Phys. Rev. B **70**, 035418 (2004)
- 7 B.S. Luk'yanchuk, M.I. Tribelsky, V. Ternovsky, J. Opt. Technol. **73**, 371 (2006)
- 8 B.S. Luk'yanchuk, V. Ternovsky, Phys. Rev. B **73**, 235432 (2006)
- 9 B.S. Luk'yanchuk, M.I. Tribelsky, V. Ternovsky, Z.B. Wang, M.H. Hong, L.P. Shi, T.C. Chong, JOPA **9** (2007) Special Issue: Nanometa Conf.
- 10 B.S. Luk'yanchuk, M.I. Tribelsky, *Anomalous Light Scattering by Small Particles and inverse hierarchy of optical resonances*, in: Collection of papers devoted to memory of Prof. M.N. Libenson, p. 101 (St. Petersburg Union of the Scientists Russia, 2005)
- 11 L.D. Landau, E.M. Lifshitz, *Electrodynamics of Continuous Media* (Butterworth-Heinemann, Oxford, 2002)
- 12 T. Okada, J. Phys. Soc. Japan. **75**, 094705 (2006)
- 13 E.D. Palik, *Handbook of Optical Constants of Solids* (Academic, New York, 1985)
- 14 U. Kreibig, M. Vollmer, *Optical Properties of Metal Clusters* (Springer, Berlin Heidelberg, 1995)